A Poroelastic Approach for Modeling Myocardial Edema in Acute Infectious Myocarditis

Wesley de Jesus Lourenço[1], Bernardo Martins Rocha[1], Ruy Freitas Reis[1], Rodrigo Weber dos Santos[1], Marcelo Lobosco[1]

[1] Federal University of Juiz de Fora, Juiz de Fora, Brazil

Abstract

Myocarditis encompasses inflammatory processes affecting the heart muscle. In 2017, more than 3 million people worldwide were affected, resulting in approximately 47,000 deaths. Although aspects of its etiology are well established, important questions remain unresolved, such as why some patients develop focal inflammation while others present diffuse patterns involving larger myocardial regions. The pathogen's role and its interaction with the immune system in disease progression also remain under debate. Addressing these questions could substantially improve patient treatment. Computational methods may contribute by elucidating pathogen–immune interactions and clarifying conditions that favor diffuse myocarditis. This work proposes a poroelastic approach to model myocardial edema in acute infectious myocarditis. A finite-deformation model is developed using partial differential equations to describe tissue displacement, fluid pressure, porosity, and pathogen and leukocyte concentrations. Key parameters are analyzed to identify conditions that may lead to diffuse myocarditis.

1. Introduction

Myocarditis, defined as inflammation of the heart muscle, affects all age groups but is more common in younger individuals, although mortality rates are higher among the elderly. Etiologies include autoimmune diseases, drug reactions, and infectious agents, with viral myocarditis being the most prevalent. In 2017, over 3 million cases were reported worldwide—a 60% increase since 1990—with annual deaths rising from 27,000 in 1990 to 47,000 in 2017. These data predate the COVID-19 pandemic, and recent studies suggesting a strong association between myocarditis and SARS-CoV-2 indicate even higher current numbers.

Identifying the precise etiology remains challenging. Endomyocardial biopsy (EMB), the gold standard diagnostic tool, is invasive. However, advances in imaging, particularly Cardiac Magnetic Resonance (CMR), have significantly improved non-invasive diagnosis by revealing myocardial edema. Increased vascular permeability during infection-induced inflammation leads to interstitial fluid accumulation, which is readily detectable on CMR.

In cases where an infectious agent is responsible for the myocarditis, the innate immune system responds to pathogens via cells such as macrophages and leukocytes, which secrete pro-inflammatory cytokines. These cytokines attract additional immune cells and increase vascular permeability, promoting leukocyte migration but also plasma leakage, resulting in edema. Within the heart, edema compromises contractility and may trigger arrhythmias, including ventricular fibrillation, which carries a risk of sudden death.

Despite these advances, major questions persist regarding disease progression: Why do some patients develop focal while others develop diffuse edema? What are the relative contributions of pathogens versus the host immune response? These uncertainties directly impact the development of therapeutic strategies. The complexity of immune dynamics, incomplete mechanistic understanding, and limitations of *in vivo* studies contribute to these gaps.

Computational modeling offers a crucial complementary approach by simulating biological processes and testing hypotheses under controlled conditions. This enables the exploration of disease progression and immune–pathogen interactions, yielding mechanistic insights that can guide therapeutic strategies.

This study investigates edema formation in myocarditis using a coupled multiphysics model that integrates poroelasticity and diffusion. Specifically, it couples immune response dynamics with interstitial fluid mechanics. The model comprises five governing equations for tissue displacement, interstitial fluid pressure, fluid fraction, and pathogen and leukocyte concentrations. Feedback mechanisms are included to couple biological and mechanical processes, accurately capturing fluid transport and immune-cell migration. The primary goal is to show that the model can qualitatively reproduce both focal and diffuse myocarditis and to identify the key factors driving

the transition from localized to widespread inflammation. To achieve this, a three-dimensional (3D) model is developed to simulate myocardial edema, comprehensively capturing immune–pathogen dynamics and tissue mechanics.

2. Mathematical Model

The mathematical formulation proposed here integrates cardiac poroelastic mechanics with immune system dynamics to simulate edema formation during myocarditis. The model couples a poroelastic subsystem with an immune subsystem through bidirectional feedback terms, enabling the emergence of focal or diffuse edema patterns.

Given the multiple scales and structural components of cardiac tissue, a continuum framework is appropriate for describing its behavior. The myocardium is modeled as a poroelastic medium fully saturated with interstitial fluid, filling the entire pore space. Through this medium, two species interact and are transported: a generic pathogen (c_p) and leukocytes (c_l). Standard continuum mechanics notation is adopted for the proposed model.

Let $\Omega \subset \mathbb{R}$, with $d = 1, 2, 3$, denote the reference configuration of a deformable porous medium. Its boundary $\partial\Omega$ is partitioned into $\Gamma \cup \Sigma$, with $\mathbf{n}$ the outward unit normal. A material point at $\mathbf{x}$ is displaced to $\mathbf{x} + \boldsymbol{u}$, with $\boldsymbol{u} : \Omega \to \mathbb{R}$. The deformation gradient is given by $\mathbf{F} = \mathbf{I} + \nabla \boldsymbol{u}, \mathbf{J} = \det \mathbf{F}$. From $\mathbf{F}$ follow the right and left Cauchy–Green deformation tensors, $\mathbf{C} = \mathbf{F}^{\mathrm{t}}\mathbf{F}$ and $\mathbf{B} = \mathbf{F}\mathbf{F}^{\mathrm{t}}$, respectively.

Fluid transport through the porous matrix follows Darcy's law. Under finite deformation, Biot's formulation [1] is employed. The first Piola–Kirchhoff stress tensor is

$$\mathbf{P} = \mathbf{P}_{\text{eff}} - \alpha \mathbf{p} \mathbf{J} \mathbf{F}^{-\mathrm{t}}, \tag{1}$$

where α is the Biot–Willis coefficient, p is pore pressure, and $\mathbf{P}_{\text{eff}}$ is the effective stress tensor derived from the strain energy density $\mathbf{P}_{\text{eff}} = \frac{\partial \mathbf{\Psi_s}}{\partial \mathbf{F}}$.

For the solid matrix (assumed incompressible), two constitutive laws are considered. The neo-Hookean (NH) model given by

$$\Psi_s^{\mathrm{NH}} = \frac{\mu_s}{2}(I_1 - d), \tag{2}$$

and the anisotropic Holzapfel–Ogden (HO) model [2]:

$$\Psi_s^{\mathrm{HO}} = \frac{a}{2b}\{\exp[b(I_1 - d)]\} + \sum_{i \in \{f,s\}} \frac{a_i}{2b_i}\{\exp[b_i(I_{4,i} - 1)^2] - 1\} + \frac{a_{fs}}{2b_{fs}}\{\exp(b_{fs} I_{8fs}^2) - 1\}. \tag{3}$$

The relevant invariants are $I_1 = \mathrm{tr}\mathbf{C}$, $I_{4,f} = \mathbf{f_0} \cdot (\mathbf{C}\mathbf{f_0})$, $I_{4,s} = \mathbf{s_0} \cdot (\mathbf{C}\mathbf{s_0})$, and $I_{8,fs} = \mathbf{f_0} \cdot (\mathbf{C}\mathbf{s_0})$. The effective stress tensor for the NH model is

$$\mathbf{P}_{\text{eff}} = \mu_{\mathbf{s}}(\mathbf{F} - \mathbf{F}^{-\mathrm{t}}) + \lambda_{\mathbf{s}} \ln(\mathbf{J}) \mathbf{F}^{-\mathrm{t}}, \tag{4}$$

with Lamé parameters μ_s and λ_s. For the HO model, it is given by

$$\mathbf{P}_{\text{eff}} = \mathbf{J}\boldsymbol{\sigma}\mathbf{F}^{\mathrm{t}} + \mathbf{z_s} \ln(\mathbf{J}) \mathbf{F}^{\mathrm{t}}, \tag{5}$$

with the Cauchy stress given by $\boldsymbol{\sigma} = \frac{1}{J}\mathbf{P}\mathbf{F}^{\mathbf{T}}$. To impose the constraint of near-incompressibility, a volumetric energy $U(J) = \frac{1}{2} z_s (\ln J)^2$ is included [3].

Since the myocardium is assumed saturated, the total volume is $V = V_f + V_s$. The solid incompressibility assumption leads to $J = 1 + \phi_f - \phi_0$, where ϕ_f is the fluid volume fraction and ϕ_0 is its reference value [1].

The poroelastic subsystem is governed by the conservation equations for displacement $\mathbf{u}$, fluid pressure p, and fluid fraction ϕ_f:

$$-\operatorname{Div}[\mathbf{P}_{\text{eff}} - \alpha \mathbf{p} \mathbf{J} \mathbf{F}^{-\mathrm{t}}] = \mathbf{0}, \tag{6a}$$

$$\rho_f \tfrac{D\phi_f}{Dt} - \tfrac{1}{J} \operatorname{Div}\Big(\phi_f \rho_f J \mathbf{F^{-1}} \tfrac{\boldsymbol{\kappa}}{\mu_{\mathbf{f}}} \mathbf{F}^{-\mathrm{t}} \nabla \mathbf{p}\Big) = \rho_f \ell(p, c_p), \tag{6b}$$

$$J - \phi_f = 1 - \phi_0. \tag{6c}$$

Here $\boldsymbol{\kappa} = \kappa_0 \mathbf{I}$ is the permeability tensor. Eq. (6a) enforces momentum balance. Eq. (6b) describes fluid mass conservation, where the source ℓ accounts for capillary and lymphatic exchange. Eq. (6c) ensures that volume changes are solely fluid-driven.

Two chemical species are transported in the interstitial fluid: pathogens (c_p) and leukocytes (c_l). Cytokines are not explicitly modeled; their effect is represented indirectly through vascular permeability changes driven by c_p and c_l. Leukocytes extravasate at rate λ_{pl}, migrate chemotactically towards the pathogen with sensitivity χ, and eliminate pathogens at rate λ_{lp}. Their reaction terms are defined as: $r_l = \lambda_{pl} c_p c_l$, and $r_p = \phi_f(\gamma_p - \lambda_{lp} c_l) c_p$, where $\gamma_p = r_p - d_p$.

The governing equations for the immune subsystem are:

$$\frac{D}{Dt}(\phi_f c_p) - \tfrac{1}{J} \operatorname{Div}(\phi_f J \mathbf{F^{-1}} \mathbf{D_p} \mathbf{F}^{-\mathrm{t}} \nabla \mathbf{c_p}) = r_p, \tag{7a}$$

$$\frac{D}{Dt}(\phi_f c_l) - \tfrac{1}{J} \operatorname{Div}(\phi_f J \mathbf{F^{-1}} \mathbf{D_l} \mathbf{F}^{-\mathrm{t}} \nabla \mathbf{c_l} - \chi \phi_f c_l J \mathbf{F^{-1}} \mathbf{F}^{-\mathrm{t}} \nabla \mathbf{c_p}) = r_l. \tag{7b}$$

If diffusion is isotropic, $\mathbf{D_p} = \mathbf{D_p}\mathbf{I}$ and $\mathbf{D_l} = \mathbf{D_l}\mathbf{I}$. For anisotropic pathogen diffusion along fibers, the tensor is given by $\mathbf{D_p} = \mathbf{D_p}\mathbf{I} + (\mathbf{D_p} - \mathbf{D_t})\mathbf{f_0} \otimes \mathbf{f_0}$.

The fluid exchange term $\ell(p, c_p)$ couples the poroelastic and immune parts, incorporating both the Starling [4] and Hill [5] mechanisms:

$$\ell(p, c_p) = C_f(c_p)\big[p_c - p - \sigma(c_p)(\pi_c - \pi_i)\big] - q_0 \left[1 + \frac{v_{\max}(p - p_0)^n}{k_m^n + (p - p_0)^n}\right], \tag{8}$$

with the filtration coefficient C_f and and the reflection coefficient σ defined as:

$$C_f(c_p) = (S/V)L_{p0}(1 + c_{bp}c_p), \tag{9}$$

$$\sigma(c_p) = \sigma_0(1 + c_{bp}c_p)^{-1}. \tag{10}$$

Here p_c is capillary pressure, π_c plasma oncotic pressure, π_i interstitial oncotic pressure, q_0 basal lymphatic flow, $v_{\max}$ maximum lymphatic flow, k_m pressure half-life, n Hill coefficient, p_0 reference interstitial pressure, L_{p0} capillary wall permeability, c_{bp} pathogen influence on permeability, and S/V surface-to-volume ratio. More details about the mathematical model and its implementation can be found in our previous papers [6, 7].

3. Numerical Results

This section presents the numerical results of myocardial edema within the human Left Ventricle (LV), focusing on two distinct scenarios: focal myocarditis and diffuse myocarditis. The simulations were performed using the coupled poroelastic and immune response model, detailed in the previous section, and a ventricular geometry segmented from a specific patient image dataset [8] using the HO model.

All computational procedures and experiments were implemented using the open-source Finite Element Method (FEM) library `FEniCS` [9]. A fixed tolerance of 10^{-6} for the residual norm (absolute or relative) was adopted as the convergence criterion in the Newton iterative scheme, and the resulting linear systems were solved using the MUMPS solver [10]. Models were discretized using tetrahedral elements in 3D. Temporal derivatives were approximated with the implicit Euler method in a monolithic approach, using a time step size of $\Delta t = 1\times10^{-1}$ day. A mixed finite element formulation was employed for the solution variables $(\mathbf{u}, \mathbf{p}, \mathbf{c_p}, \mathbf{c_l}, \phi_\mathbf{f})$. Specifically, the displacement $(\mathbf{u})$ and fluid fraction (ϕ_f) were approximated with the MINI element [11], while Lagrange linear elements were used for the scalar variables c_p, c_l, and p.

Simulations were executed on a cluster equipped with an AMD EPYC 7713 and 528GB RAM (running Rocky Linux 9.3). Codes were written in Python (v3.8.10) with FEniCS 2019.2, and results were post-processed using Paraview. The full set of parameters used in the simulations can be found in our previous work [6]. Table 1 summarizes the key parameter values identified to distinguish between focal and diffuse myocarditis.

Error control in complex multiphysics problems remains challenging [12, 13]. While some works utilize the increment norm [12], others prefer the residual norm [13]. Here, the residual norm was chosen, as vanishing increments may reflect solution stagnation rather than true convergence.

Figure 1 illustrates the simulated fluid phase results in focal (left) and diffuse (right) myocarditis. Each line represents the evolution of fluid phase values at distinct spatial points over time, demonstrating the dynamics induced by myocarditis.

Table 1. Parameter values used to represent focal and diffuse myocarditis in 3D simulations.

Parameter	Unit	Focal 3D	Diffuse 3D
D_p	cm^2/d	5×10^{-4}	1×10^{-3}
D_l	cm^2/d	5×10^{-1}	3×10^{-2}
λ_{pl}	$1/d\ (cell/cm^3)$	1.2×10^{-1}	5×10^{-2}
γ_p	$1/d$	9×10^{0}	6×10^{-2}

Our simulations highlight that the mechanical properties of the tissue, the efficiency of the immune response, and the characteristics of the pathogen jointly govern the dynamics of myocarditis and edema formation. In particular, we observed that the ratios λ_{lp}/γ_p (phagocytosis-to-pathogen reproduction ratio) and D_l/D_p (leukocyte-to-pathogen mobility ratio) facilitate the widespread diffusion of both the pathogen and the resulting edema in the heart.

The diffuse edema formation in the LV was found to follow the propagation of a 3D pathogen wave (not explicitly shown in the Figure) that originated from a small initial infected region. This wave traveled through the cardiac tissue until it collided with itself and eventually vanished. The presence of pathogens locally induces the entry of leukocytes and fluid into the interstitial space of the tissue. As this pathogen wave sweeps across the heart, diffuse edema emerges. This spatiotemporal pattern strongly suggests the existence of a nonlinear reaction-diffusion wave, a phenomenon typically observed in complex biological systems.

While the propagation of the pathogen front likely depends on pathogen diffusion and replication, the wave tail is primarily governed by diffusion and leukocyte efficiency in pathogen elimination. However, sensitivity analysis further revealed that other tissue characteristics, such as stiffness, also significantly impact diffuse edema formation [6]. The clear characterization of this nonlinear wave, identified in the development of diffuse edema using the proposed model, warrants further dedicated investigation in future studies.

4. Conclusion

This work presented a poroelastic model to investigate edema formation in acute infectious myocarditis, coupling cardiac tissue mechanics with immune-pathogen interactions. The simulations reproduced both focal and diffuse edema, showing that tissue stiffness, pathogen dynamics, and immune efficiency play central roles in disease

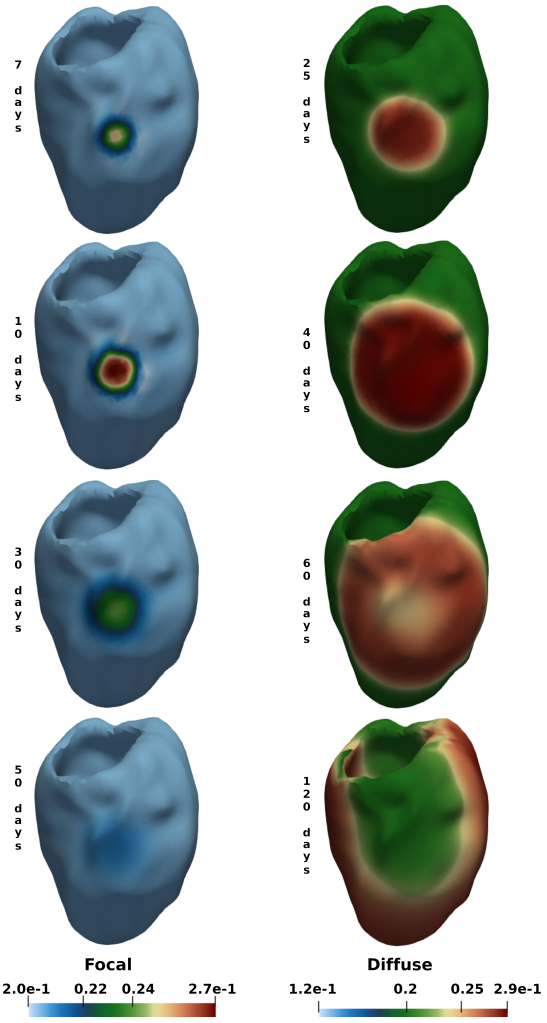

Figure 1. Evolution of interstitial fluid phase ϕ_f over time points for (left) focal myocarditis and (right) diffuse myocarditis, illustrating the difference in dynamics and spread between the two conditions.

progression. In particular, the emergence of diffuse myocarditis was associated with the propagation of nonlinear pathogen waves through the myocardium. These findings highlight the potential of computational modeling to improve the mechanistic understanding of myocarditis and to support the development of new therapeutic strategies. Future work will focus on further characterizing the nonlinear dynamics observed and extending the model to integrate additional biological pathways.

Acknowledgments

This work has been supported by UFJF, by CAPES - Finance Code 001; by CNPq - Grant number 423278/2021-5, 308117/2025-5, and 301120/2025-0; and by FAPEMIG Grant number APQ-02513-22 and PCE-00048-25; by FINEP SOS Equipamentos 2021 AV02 0062/22.

References

[1] MacMinn CW, Dufresne ER, Wettlaufer JS. Large deformations of a soft porous material. Phys Rev Appl 2016; 5(4):044020(30).

[2] Nash MP, Hunter PJ. Computational mechanics of the heart. From tissue structure to ventricular function. J Elasticity 2000;61(1-3):113–141.

[3] Zheng P, Zhang K. On the effective stress law and its application to finite deformation problems in a poroelastic solid. Int J Mech Sci 2019;161-162:e105074.

[4] Starling EH. On the absorption of fluids from the connective tissue spaces. J Physiol 1896;19(4):312–326.

[5] Keener JP, Sneyd J. Mathematical physiology, volume 8. Springer, 1998.

[6] Lourenço WdJ, Reis RF, Ruiz-Baier R, Rocha BM, dos Santos RW, Lobosco M. A poroelastic approach for modelling myocardial oedema in acute myocarditis. Front Physiol July 2022;13.

[7] Barnafi NA, Gómez-Vargas B, Lourenço WJ, Reis RF, Rocha BM, Lobosco M, Ruiz-Baier R, dos Santos RW. Finite element methods for large-strain poroelasticity/chemotaxis models simulating the formation of myocardial oedema. J Sci Comput July 2022;92(3).

[8] Warriner DR, Jackson T, Zacur E, Sammut E, Sheridan P, Hose DR, Lawford P, Razavi R, Niederer SA, Rinaldi CA, Lamata P. An asymmetric wall-thickening pattern predicts response to cardiac resynchronization therapy. JACC Cardiovasc Imag 2018;11(10):1545–1546.

[9] Alnæs MS, Blechta J, Hake J, Johansson A, Kehlet B, Logg A, Richardson C, Ring J, Rognes ME, Wells GN. The FEniCS project version 1.5. Arch Numer Software 2015; 3(100):9–23.

[10] Amestoy PR, Duff IS, L'Excellent JY, Koster J. Mumps: a general purpose distributed memory sparse solver. In International Workshop on Applied Parallel Computing. Springer, 2000; 121–130.

[11] Arnold DN, Brezzi F, Fortin M. A stable finite element for the stokes equations. Calcolo 1984;21(4):337–344.

[12] Borregales M, Radu FA, Kumar K, Nordbotten JM. Robust iterative schemes for non-linear poromechanics. Comput Geosci 2018;22(4):1021–1038.

[13] White JA, Castelletto N, Klevtsov S, Bui QM, Osei-Kuffuor D, Tchelepi HA. A two-stage preconditioner for multiphase poromechanics in reservoir simulation. Comput Methods Appl Mech 2019;357:112575.

Address for correspondence:

Marcelo Lobosco PPGMC, Campus Universitário, Rua José Lourenço Kelmer, s/n - São Pedro, Juiz de Fora - MG, 36036-900

marcelo.lobosco@ufjf.br